Real-world Quantum Sensors: Evaluating Resources for Precision Measurement

N. L. Thomas-Peter,[*] Brian J. Smith, and I. A. Walmsley

Clarendon Laboratory, University of Oxford,

Parks Road, Oxford OX1 3PU, United Kingdom

U. Dorner

Centre for Quantum Technologies, National University of Singapore,

3 Science Drive 2, 117543 Singapore, Singapore and

Clarendon Laboratory, University of Oxford,

Parks Road, Oxford OX1 3PU, United Kingdom

(Dated: December 31, 2010)

Abstract

Quantum entanglement enables measurements with precision beyond what is possible classically, ideally attaining the Heisenberg limit. Enumerating the resources required to reach a specified precision is key to deciding whether the classical bound has been breached. We address this question for a real-world quantum sensor of optical phase by demonstrating a scalable scheme for generating heralded photonic Holland-Burnett states [1], characterized by full quantum state tomography. These entangled states exhibit Heisenberg scaling and show near optimal loss-tolerance [2, 3]. The sensor performance is quantified by the quantum Cramér-Rao bound (QCRB), the best precision that can be achieved with the actual prepared state, independent of detector configuration. We then show how the commonly applied measures of super-resolution and super-sensitivity [4] compare to the QCRB and demonstrate that post-selection can provide an artificial precision enhancement. This analysis allows us to place limits on the sensor parameters required for operation beyond the classical limit.

---

[*]Electronic address: n.thomas-peter1@physics.ox.ac.uk

An important class of quantum-enhanced technologies involves sensing, in which a quantum probe is used to measure parameters of another physical system [5]. Such sensors are ubiquitous for gathering information about systems from gravitational waves to tenuous molecular gases. Entangled states of multiple particles are a critical resource to enable quantum enhancement [6], as are detectors that implement optimal measurements [7]. The cost of such resources provides a basis for deciding whether the quantum device outperforms its classical counterpart. In realistic experimental implementations, where loss and noise are unavoidable, heralded or deterministic input probe preparation is necessary to ensure accurate resource accounting. Aside from potentially yielding a distorted impression of the cost of a measurement, poor accounting may be problematic when the system being probed is degraded by absorbing any energy from the input state, for example, a Bose-Einstein condensate or fragile biological system. In these situations, practical sensing strategies must involve noise- and loss-tolerant probe states to enable quantum enhancement even in the presence of realistic experimental imperfections. Furthermore, the QCRB is reached only when optimal measurements are performed [7]. Therefore, attention must be paid both to preparing a state that reaches the Heisenberg limit, and to measurements that extract maximum information from that state, saturating the QCRB.

Here we consider a sensor based on optical interferometry. We evaluate the cost, in terms of time and photon number, of reaching a given precision in an estimate of the phase, ϕ, between two modes of a light field. To estimate ϕ, an input probe is prepared in state $\hat{\rho}$, which evolves into the state $\hat{\rho}(\phi)$ by interaction with the phase-shifting element in the interferometer. A measurement on $\hat{\rho}(\phi)$ is performed at the sensor output. This is repeated ν times and ϕ is estimated from the ν measurement outcomes. We employ an optical sensor design based on a heralded two-photon Holland-Burnett (HB) state that, in principle, attains a QCRB with Heisenberg scaling. It is the simplest configuration that exhibits a quantum enhancement, providing the least stringent constraints on sensor transmissivity and decoherence as well as allowing assessment of the impact of real-world imperfections on precision measurement.

The scheme used to generate heralded HB states is shown in Fig. 1a. A polarisation based N-photon HB state is obtained by combining two orthogonally polarised $N/2$-photon Fock states at a polarizing beam splitter. The required Fock states are generated by two parametric downconverters (PDC), where $N/2$ photons in one mode of each PDC are heralded by

detection of $N/2$ photons in the other mode. The PDCs are designed to produce spectrally disentangled modes [8] so that heralding does not compromise the state purity, which is crucial for high-visibility interferometry. Since spectral filtering is not required to increase the state purity, the preparation efficiency is determined solely by the system loss. In principle this source, with the use of photon-number-resolving heralding detectors [9], generates a perfect HB state of arbitrary N. Furthermore, the optimal detection arrangement for these states is experimentally feasible.

The quality of the heralded Fock states used to generate the HB state were tested by means of Hong-Ou-Mandel interference between heralded single photons (Fig. 2a). The theoretical fit gives a visibility of $90 \pm 3\%$ ($80 \pm 3\%$ raw) and sets a lower bound on the input photon purity and distinguishability. The residual impurity is partly intrinsic [8] and partly due to imperfect compensation of the optical fiber birefringence.

The heralded HB states are launched into a polarisation Mach-Zehnder interferometer (PMZI in Fig. 1b), which introduces a controllable relative phase, ϕ (see Appendix A) between the two modes. Figure 2b shows the detection count-rate phase-dependence for heralded single-photon states (dashed) and heralded two-photon HB states (solid). The theoretical fits show visibilities of $90.9 \pm 0.5\%$ for the single-photon and $80.6 \pm 1.5\%$ ($76.4 \pm 1.4\%$ raw) for the HB state. The latter is consistent with the measured state purity.

In general, the precision of the phase estimate for a given sensor configuration is limited by the Cramér-Rao bound (CRB) [7], $\Delta\phi \geq 1/\sqrt{\nu F(\phi)}$, where

$$F(\phi) = \sum_j \frac{1}{p_j(\phi)} \left| \frac{\partial p_j(\phi)}{\partial \phi} \right|^2, \tag{1}$$

is the Fisher information (FI). The probabilities $p_j(\phi) = \text{Tr}(\hat{\rho}(\phi)\hat{\Pi}_j)$ correspond to a particular outcome j of a measurement described by a set of measurement operators $\{\hat{\Pi}_j\}$. The CRB is achieved for large ν with maximum likelihood estimation [10]. $F(\phi)$ is bounded from above by the quantum Fisher information (QFI), F_Q, found by maximising $F(\phi)$ over all physical measurement operator sets. Hence the quantum Cramér-Rao bound (QCRB), $\Delta\phi \geq 1/\sqrt{\nu F_Q(\phi)}$, depends only on the input state and is independent of the specific detector configuration [7].

Ideally, the QCRB of N uncorrelated photons leads to the standard quantum limit $\Delta\phi \geq \Delta\phi_{\text{SQL}} = 1/\sqrt{\nu N}$. However, if the sensor has finite transmissivity η, this becomes the standard interferometric limit (SIL) $\Delta\phi \geq \Delta\phi_{\text{SIL}} = 1/\sqrt{\nu \eta N}$ [2].

The Heisenberg limit $\Delta\phi \geq \Delta\phi_{\mathrm{HL}} = 1/\sqrt{\nu}N$ is saturated by the widely studied 'N00N state' [4, 11–24]. This state is very susceptible to loss; removal of even a single photon results in a state insensitive to phase. The QFI is therefore scaled by the probability that all photons are transmitted, η^N, and the QCRB becomes $\Delta\phi \geq 1/\sqrt{\nu\eta^N}N$. Alternatively, this can be interpreted as requiring $\nu' = \nu/\eta^N$ successful trials (i.e. a measurement time that grows exponentially in N) to reach the same level of precision as in the lossless case (see Appendix B).

By comparison, the QCRB of a HB state in the lossless case is $\Delta\phi \geq 1/\sqrt{\nu N(N/2 + 1)}$ which, for large N, has Heisenberg scaling that differs only by a constant factor. With loss this state retains phase sensitivity and precision enhancement far better than N00N states [3]. Indeed, the QCRB for the HB state approximately follows the optimum value for moderate η and moderate N [2].

For $N = 2$, HB and N00N states are equivalent and their associated optimal measurement is a projection onto $|\Psi_\pm\rangle = (|2,0\rangle \pm |0,2\rangle)/\sqrt{2}$, where $|m,n\rangle$ denotes m (n) diagonally (anti-diagonally) polarised photons. This measurement set has three possible outcomes: $j = \pm$ (detection of $|\Psi_\pm\rangle$) and $j = 0$ (otherwise). In practice, it is difficult to realise single-mode sensors and the measurement outcomes typically have probabilities $p_\pm(\phi) = f[1 \pm V\cos(2\phi)]/2$ and $p_0(\phi) = 1 - p_+(\phi) - p_-(\phi)$, leading to a bound $\Delta\phi \geq \Delta\phi_{\mathrm{min}} = 1/\sqrt{\nu f}NV$ (see Appendix B). Here, $f = \eta_{\mathrm{p}}\eta^2$ where η_{p}, the preparation efficiency, is the proportion of the input state which can lead to a two-click detection event; η^2 is the probability that two photons are transmitted through the sensor and successfully registered; V is the interference visibility accounting for imperfect state preparation and detectors. Multimode states and measurements may lead to non-ideal interference because of unmeasured distinguishing information. The state is said to exhibit super-resolution if $p_\pm(\phi)$ oscillates at twice the applied phase. For larger N, super-resolution requires oscillations of N times the applied phase. To surpass the SIL requires $\Delta\phi_{\mathrm{min}} < \Delta\phi_{\mathrm{SIL}}$, leading to a threshold visibility $V_{\mathrm{th}} = \sqrt{\eta/fN}$. A state is said to exhibit super-sensitivity if $V \geq V_{\mathrm{th}}$ [4].

This analysis is commonly applied in post-selection where only data resulting in N-photon outcomes are recorded. Then η and f are set to 1, and N is the number of photons detected. For the two-photon case, this yields a threshold visibility $V_{\mathrm{th}} = 1/\sqrt{2}$. The measured HB-state fringe visibility (Fig. 2b) significantly exceeds this bound and so, by this analysis, we achieve super-sensitivity. Heralding, however, affords a more complete reckoning of the

4

resources consumed by counting all photons input into the interferometer, since f and η can then be estimated experimentally. f is determined from the ratio of four-fold coincidences to heralding events, giving $f = 0.0161 \pm 0.0003$. Assuming that heralding ensures two photons are initially present ($\eta_p = 1$) implies $f = \eta^2$. This results in $V_{th} = \sqrt{\eta/Nf} = 1.99$, an unphysical visibility, demonstrating that this configuration cannot beat the SIL. Thus we conclude that for a quantum sensor with real-world imperfections, measures of quantum enhancement based on post-selection can underestimate the resources required to obtain a given precision.

The above discussion considers post-selecting on events where only two photons are detected. As previously discussed, this ignores any information that may be present in the lower photon-number subspaces. More importantly, to calculate the QCRB for the heralded state and to compare it to the SIL requires the complete density matrix. This is obtained by state tomography using the experimental arrangement shown in Fig. 1c [25] (see Appendix A). Population in lower photon number subspaces arises from loss, meaning that coherences between subspaces of different photon number are zero.

Figure 3 shows the reconstructed density matrix. The heralded state has populations of 0.686, 0.277, and 0.037 in the zero-, one-, and two-photon subspaces respectively. It also has an average photon number of 0.35 and $F_Q = 0.104$, giving a QCRB $\Delta\phi \geq 3.11/\sqrt{\nu}$. We compare this with the CRB of the post-selected state, $\Delta\phi \geq 3.24/\sqrt{\nu}$. This demonstrates that post-selecting can discard useful information. Furthermore, for a classical state with the same average input photon number as the reconstructed state we have $\Delta\phi_{SQL} = 1.69/\sqrt{\nu}$, showing that, according to the QCRB, the SQL cannot be surpassed.

To go beyond the classical performance limit with realistic quantum sensors requires stringent bounds on sensor throughput as well as probe-state preparation and detection efficiencies. For heralded $N00N$ states, $f = \eta_p \eta^N$ must satisfy

$$f \geq \eta/NV^2, \tag{2}$$

(see Appendix B). For the ideal two-photon situation ($\eta_p = V = 1$), where HB and $N00N$ states are equivalent, this implies $\eta \geq 1/2$. This benchmark for heralded two-photon states, which includes detector efficiencies and sensor transmissivity, provides a challenging goal that must be achieved to surpass the classical limit and which has not yet been achieved.

Quantum photonics using feasible laboratory technology holds great promise for per-

formance beyond the classical domain. Here we have demonstrated a scalable method to generate heralded entangled states of light for precision phase estimation, a key step to demonstrating a real-world improvement over the SQL. By fully characterizing this source we have calculated the ultimate precision that can be obtained and in doing so we have put bounds on the sensor parameters required in order for quantum technologies to be viable.

---

[1] Holland, M. J. & Burnett, K. Interferometric detection of optical phase shifts at the Heisenberg limit. *Physical Review Letters* **71**, 1355–1358 (1993).

[2] Dorner, U. *et al.* Optimal quantum phase estimation. *Physical Review Letters* **102**, 040403 (2009).

[3] Dunningham, J. A., Burnett, K. & Barnett, S. M. Interferometry below the standard quantum limit with Bose-Einstein condensates. *Physical Review Letters* **89**, 150401 (2002).

[4] Resch, K. J. *et al.* Time-reversal and super-resolving phase measurements. *Physical Review Letters* **98**, 223601 (2007).

[5] Giovannetti, V., Lloyd, S. & Maccone, L. Quantum-enhanced measurements: Beating the standard quantum limit. *Science* **306**, 1330–1336 (2004).

[6] Giovannetti, V., Lloyd, S. & Maccone, L. Quantum metrology. *Physical Review Letters* **96**, 010401 (2006).

[7] Braunstein, S. L. & Caves, C. M. Statistical distance and the geometry of quantum states. *Physical Review Letters* **72**, 3439–3443 (1994).

[8] Mosley, P. J. *et al.* Heralded generation of ultrafast single photons in pure quantum states. *Physical Review Letters* **100**, 133601 (2008).

[9] Achilles, D., Silberhorn, C., Śliwa, C., Banaszek, K. & Walmsley, I. A. Fiber-assisted detection with photon number resolution. *Opt. Lett.* **28**, 2387–2389 (2003).

[10] Braunstein, S. L. Quantum limits on precision measurement of phase. *Physical Review Letters* **69**, 3598 (1992).

[11] Sanders, B. C. & Milburn, G. J. Optimal quantum measurements for phase estimation. *Physical Review Letters* **75**, 2944–2947 (1995).

[12] Bollinger, J. J., Itano, W. M. & Wineland, D. J. Optimal frequency measurements with maximally correlated states. *Physical Review A* **54**, R4649–R4652 (1996).

[13] Boto, A. N. *et al.* Quantum interferometric optical lithography: Exploiting entanglement to beat the diffraction limit. *Physical Review Letters* **85**, 2733–2736 (2000).

[14] Mitchell, M. W., Lundeen, J. S. & Steinberg, A. M. Super-resolving phase measurements with a multiphoton entangled state. *Nature* **429**, 161–164 (2004).

[15] Eisenberg, H. S., Hodelin, J. F., Khoury, G. & Bouwmeester, D. Multiphoton path entanglement by nonlocal bunching. *Physical Review Letters* **94**, 090502 (2005).

[16] Higgins, B. L., Berry, D. W., Bartlett, S. D., Wiseman, H. M. & Pryde, G. J. Entanglement-free Heisenberg-limited phase estimation. *Nature* **450**, 393–396 (2007).

[17] Resch, K. J. *et al.* Entanglement generation by fock-state filtration. *Physical Review Letters* **98**, 203602 (2007).

[18] Nagata, T., Okamoto, R., O'Brien, J. L., Sasaki, K. & Takeuchi, S. Beating the standard quantum limit with four-entangled photons. *Science* **316**, 726–729 (2007).

[19] Smith, B. J., Mosley, P. J., Lundeen, J. S. & Walmsley, I. A. Heralded generation of two-photon noon states for precision quantum metrology. In *Conference on Lasers and Electro-optics & Quantum Electronics and Laser Science Conference*, vol. 1-9, 3044–3045 (2008).

[20] Smith, B. J., Kundys, D., Thomas-Peter, N. L., Smith, P. G. R. & Walmsley, I. A. Phase-controlled integrated photonic quantum circuits. *Optics Express* **17**, 13516–13525 (2009).

[21] Matthews, J. C. F., Politi, A., Stefanov, A. & O'Brien, J. L. Manipulation of multiphoton entanglement in waveguide quantum circuits. *Nature Photonics* **3**, 346–350 (2009).

[22] Kim, H., Park, H. S. & Choi, S.-K. Three-photon n00n states generated by photon subtraction from double photon pairs. *Optics Express* **17**, 19720–19726 (2009).

[23] Afek, I., Ambar, O. & Silberberg, Y. High-noon states by mixing quantum and classical light. *Science* **328**, 879–881 (2010).

[24] Matthews, J. C. F., Politi, A., Bonneau, D. & O'Brien, J. L. Heralded entanglement for quantum enhanced measurement with photons. *arXiv:quant-ph* (2010). URL `http://arxiv.org/abs/1005.5119v1`.

[25] Thomas-Peter, N. L., Smith, B. J. & Walmsley, I. A. Tomography of a heralded N00N state with losses. In *Conference on Lasers and Electro-optics & Quantum Electronics and Laser Science Conference*, vol. 1-9, 2430–2431 (2009).

[26] Adamson, R. B. A., Shalm, L. K., Mitchell, M. W. & Steinberg, A. M. Multiparticle state tomography: Hidden differences. *Physical Review Letters* **98**, 043601 (2007).

[27] Banaszek, K., D'Ariano, G. M., Paris, M. G. A. & Sacchi, M. F. Maximum-likelihood estimation of the density matrix. *Physical Review A* **61**, 010304(R) (1999).

Appendix A: Heralded Holland-Burnett state generation

The heralded HB-state source is based upon generation of heralded Fock states by means of parametric downconversion in Potassium Dihydrogen Phosphate (KDP) [8]. A crucial feature of this nonlinear source is that the modes are entangled only in photon number and have no entanglement in any other degrees of freedom. This allows detection of N photons in one mode to herald, in principle, N photons in the other mode in a pure spatiotemporal quantum state. No spectral filtering is needed to increase the state purity of the heralded photons. This scheme is therefore scalable, since there is no decrease in heralding efficiency arising from discarding photons by filtration. The use of high-efficiency number-resolving heralding detectors enables production of precisely the target HB state abrogating the need for ancillary assumptions about contamination from higher or lower photon numbers.

A mode-locked Ti:Sapphire laser system operating at 80 MHz provides 100 fs duration pulses centered at a wavelength of 830 nm. These pulses are frequency doubled in Beta Barium Borate (BBO) to a wavelength of 415 nm. After filtering any residual infrared radiation, the UV-pulses are used to concurrently pump two KDP crystals oriented for type-II collinear parametric downconversion (PDC) [8]. The orthogonally polarised PDC modes are split using polarizing beam splitters. The vertically polarised mode of each PDC source is detected by a fiber-coupled avalanche photodiode (APD) serving as a herald signal for the horizontal modes. After rotating one of the horizontal modes to vertical polarisation, the heralded modes are sent to a fiber-coupled polarizing beam splitter (FPBS) where they are combined

into a single spatial mode. Each heralded beam and the FPBS output are passed through polarisation compensation wave plates to ensure appropriate polarisation after passing through the optical fibers. The FPBS output has additional polarisation compensation. Successful preparation of the heralded state is signaled by a coincidence detection event between these two heralding detectors. When only one photon is registered at each herald detector, this heralds the state $|1, 1\rangle_{\mathrm{HV}})$ where $|n, m\rangle_{\mathrm{HV}}$ denotes n (m) horizontally (vertically) polarised photons. This is equivalent to the two-photon HB state $(|2, 0\rangle_{+-} - |0, 2\rangle_{+-})/\sqrt{2}$, where $+, -$ denotes the $45°$ rotated basis. Note that single photons are typically heralded with an efficiency of 0.18 in this experimental configuration.

Interferometry

We used a polarisation-based interferometer to apply phase shifts between $+45°$ and $-45°$ plane polarisation modes. This consists of a half-wave plate situated between two quarter-wave plates. The quarter-wave plates were initially aligned to rotate $+$ into $-$ without the half-wave plate. The addition of the half-wave plate allows application of the phase, ϕ, being twice the angle of the half-wave plate. The $+$ and $-$ modes are then interfered on a polarizing beam splitter for analysis.

State tomography of the heralded state

We characterize the polarisation and photon number degrees of freedom of the heralded state by performing state tomography [25, 26]. A half- (HWP) is followed by a quarter-wave plate (QWP), the angles of which determine the measurement implemented. The HWP and QWP are followed by a polarizing beam splitter (PBS) with the transmitted mode coupled into a single mode fiber-coupled APD and the reflected mode coupled into a single-mode fiber beam splitter (50:50) with outputs connected to fiber-coupled APDs. This allows partial photon number resolution, giving information about the different photon number subspaces when measured in coincidence with the herald signal. The wave plate settings used, $\{\theta, \phi\}$, were $\{0, 0\}$, $\{0, 11.25\}$, $\{0, 22.5\}$, $\{0, 45\}$, $\{22.5, 0\}$, $\{22.5, 22.5\}$, $\{22.5, 45\}$, and $\{45, 22.5\}$, where θ and ϕ are the angles of the QWP and HWP respectively. This forms an over-complete set of measurements on the whole space. The state was reconstructed by

maximum likelihood estimation [27] using the measurement outcomes. In order to check the consistency of the reconstructed density matrix, we calculate an overlap of 0.85 of the two-photon subspace with the ideal two-photon HB state, Fig. 3c, in agreement with the Hong-Ou-Mandel interference visibility.

Appendix B: Fisher Information and Phase Uncertainty

The amount of information about the phase ϕ between two modes (polarisation in our case) that can be extracted by a given experimental configuration is quantified by the Fisher information

$$F(\phi) = \sum_j \frac{1}{p_j(\phi)} \left| \frac{\partial p_j(\phi)}{\partial \phi} \right|^2, \tag{B1}$$

where the probabilities $p_j(\phi)$ correspond to a particular outcome j of a measurement described by a set of operators $\{\hat{\Pi}_j\}$ when the actual parameter to be estimated has a value ϕ. The precision with which ϕ can be estimated is determined by the Cramér-Rao bound (CRB),

$$\Delta\phi \geq 1/\sqrt{\nu F(\phi)}, \tag{B2}$$

which can be achieved for a large number of trials ν and an unbiased estimator, such as a maximum likelihood method. The CRB is bounded from below by the quantum Cramér-Rao bound (QCRB), which is independent of the measurement and depends only on the state used,

$$\Delta\phi \geq 1/\sqrt{\nu F(\phi)} \geq 1/\sqrt{\nu F_Q(\phi)}, \tag{B3}$$

where $F_Q(\phi) = F_Q(\hat{\rho}(\phi))$ is the quantum Fisher information.

In a realistic experiment an N-photon detection event, which would ideally signal projection onto a two-mode $N00N$ state, is realised with a probability determined by the generalised measurement operators

$$\hat{\Pi}_\pm = \sum_\lambda \hat{P}_\pm^{(\lambda)}, \tag{B4}$$

where $\{\hat{P}_\pm^{(\lambda)}\}$ are a set of projection operators onto two-mode $\pm N00N$ states, $|\Psi_\pm\rangle_\lambda = (|N,0\rangle_\lambda \pm |0,N\rangle_\lambda)/\sqrt{2}$. Here, λ denotes experimentally inaccessibly degrees of freedom (e.g. spectral modes) which provide distinguishing information and $|m,n\rangle_\lambda$ are states with

m photons in one polarisation mode and n photons in the other. The probability of an N-photon detection event is then

$$p_\pm(\phi) = \mathrm{Tr}\left(\hat{\rho}(\phi)\hat{\Pi}_\pm\right), \tag{B5}$$

and probability $p_0(\phi) = 1 - p_+(\phi) - p_-(\phi)$ that no detection event is registered. In the most common cases, where the input state consists of more than one space-time mode containing correlated photons, $p_\pm(\phi)$ takes the form:

$$p_\pm(\phi) = f[1 \pm V\cos(N\phi)]/2, \tag{B6}$$

where f and V both depend upon the presence of distinguishing information in the input state. Note that the different projectors, $\hat{\Pi}_\pm$, are realised by variation of a known reference phase in the interferometer. The Fisher information for this configuration is given by

$$F(\phi) = fN^2V^2\frac{\sin^2(N\phi)}{1 - V^2\cos^2(N\phi)}, \tag{B7}$$

where we have made use of the first derivatives of $p_\pm(\phi)$ with respect to ϕ,

$$\frac{\partial p_\pm(\phi)}{\partial\phi} = \mp\frac{f}{2}NV\sin(N\phi). \tag{B8}$$

Note that the denominator in Eq. (B7) is greater than or equal to $\sin^2(N\phi)$ for $0 \le V \le 1$, which sets a bound on the Fisher information,

$$F(\phi) \le fV^2N^2. \tag{B9}$$

The phase uncertainty that can be achieved with ν trials is then bounded by the Cramér-Rao bound

$$\Delta\phi \ge 1/(\sqrt{\nu f}NV). \tag{B10}$$

Comparison with the precision that can be achieved in a classical approach with N particles, i.e. the standard quantum limit (SQL),

$$\Delta\phi_{\mathrm{SQL}} = 1/\sqrt{\nu N}, \tag{B11}$$

implies that in order to demonstrate precision beyond the SQL,

$$V \ge 1/\sqrt{fN}. \tag{B12}$$

11

Effects of loss on measurement precision

We consider the case of a single spectral-mode (λ) sensor, since this enables f to be calculated straightforwardly and allows comparison with previous work involving super-resolution and super-sensitivity criteria. For the case of no loss, we define $f = \eta_\mathrm{p}$, the production efficiency of the single-mode $N00N$ state. When there is balanced loss in the interferometer, characterized by the transmissivity η, the probability that an N-photon $N00N$ state is successfully detected is decreased by a factor η^N, giving $f = \eta_p \eta^N$. In the classical case, the probability that a coherent state is transmitted is simply η so that the classical phase uncertainty is bounded by $\Delta\phi_{\mathrm{SIL}} = 1/\sqrt{\nu\eta N}$.

Heralding a perfect $N00N$ state means that $\eta_p = 1$ and f can be estimated from the ratio of successful $N00N$ detection events to herald events, giving the channel transmission $\eta = \sqrt[N]{f/\eta_p}$. To surpass the performance allowed classically, i.e. $\Delta\phi_{\mathrm{SIL}} \geq 1/(\sqrt{\nu f}VN)$, the fringe visibility must be

$$V \geq \sqrt{\frac{\eta}{fN}}. \tag{B13}$$

Another way to view this is that the system transmissivity is bounded by the intrinsic source efficiency η_p, $N00N$-state photon number N, and fringe visibility. This limit is determined from Eq. (B13) by substituting $\eta_p \eta^N = f$ and solving for η, which gives

$$\eta \geq \left(\eta_p N V^2\right)^{1/(1-N)}. \tag{B14}$$

Quantum Fisher Information of the Reconstructed State

For the reconstructed density matrix in our experiment, the quantum Fisher information is given by

$$F_Q = 2\sum_{k,l} \frac{(p_k - p_l)^2}{p_k + p_l} |\langle\xi_k|\hat{n}|\xi_l\rangle|^2, \tag{B15}$$

where $\hat{n}$ is the photon number operator in the sensor arm of the interferometer, and $\{p_k\}$ and $\{|\xi_k\rangle\}$ are the eigenvalues and corresponding eigenvectors of the reconstructed density matrix.

Time required to achieve equal precision: Classical and Post-Selection

To calculate the time it takes for a post-selected scheme to achieve the same level of precision as a classical scheme when losses are present, we assume that both experiments are run at a rate of γ. In this case the phase uncertainties for the classical and post-selected $N00N$ state are bounded by

$$\Delta\phi_{\mathrm{c}} = 1/\sqrt{\nu_{\mathrm{c}}N}, \tag{B16}$$

and

$$\Delta\phi_{\mathrm{N00N}} = 1/\sqrt{\nu_{\mathrm{N00N}}\eta_{\mathrm{p}}V^2N^2}, \tag{B17}$$

where $\nu_{\mathrm{c}} = \gamma T_{\mathrm{c}}$ and $\nu_{\mathrm{N00N}} = \gamma T_{\mathrm{N00N}}$ are the number of successful detection events in the classical and post-selected cases. Setting Eqs. (B16) and (B17) equal leads to a constraint on the number of post-selected trials necessary

$$\nu_{\mathrm{N00N}} = \frac{\nu_{\mathrm{c}}}{\eta_{\mathrm{p}}V^2N}. \tag{B18}$$

The time required to register $\nu_{\mathrm{c(N00N)}}$ classical (post-selected $N00N$) events when losses are present is $T_{\mathrm{c}} = \nu_{\mathrm{c}}/(\eta\gamma)$ ($T_{\mathrm{N00N}} = \nu_{\mathrm{N00N}}/(\eta^N\gamma)$), which stems from a decreased rate of successful detection events by the transmission probability η (η^N). Dividing both sides of Eq. (B18) by $\eta^N\gamma$, giving T_{N00N} on the left-hand side, we obtain

$$T_{\mathrm{N00N}} = \frac{T_{\mathrm{c}}}{\eta^N}\frac{\eta}{\eta_{\mathrm{p}}NV^2}, \tag{B19}$$

which shows that the time taken to collect sufficient data with the post-selection approach to give a precision equal to a classical scheme grows exponentially with the number of post-selected photons.
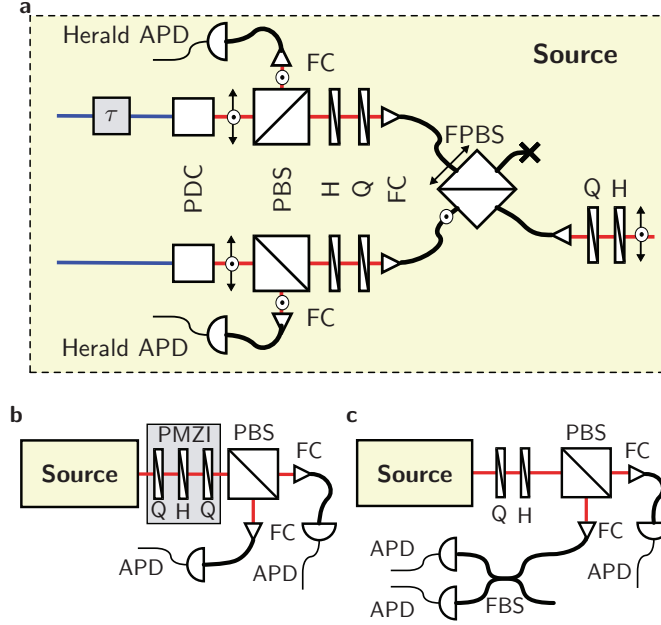
FIG. 1: **Setup for generation and characterization of heralded Holland-Burnett states. a** Scalable HB state generation based on two parametric downconverters (PDC) (see Appendix A). A half- (H) and a quarter-wave plate (Q) after each PDC adjust the polarisations to combine the photons at a fiber polarizing beam splitter (FPBS). A coincidence detection event between the heralding avalanche photodiodes (Herald APDs) signals the presence of the two-photon HB state at the output of the FPBS. **b** A polarisation Mach-Zehnder interferometer (PMZI) applies a phase ϕ between $\pm45°$ rotated polarisation modes. Coincidence detection events between the avalanche photodiodes (APD) implement the optimal measurement for the two-photon HB state. **c** Tomographic measurements are implemented using a quarter- (Q) and half-wave plate (H) combination followed by a polarizing beam splitter (PBS). Outputs are coupled into single-mode fiber (FC) with the reflected mode split by a 50:50 fiber beam splitter (FBS) to allow partial number resolution. All outputs are detected using avalanche photodiodes (APD).
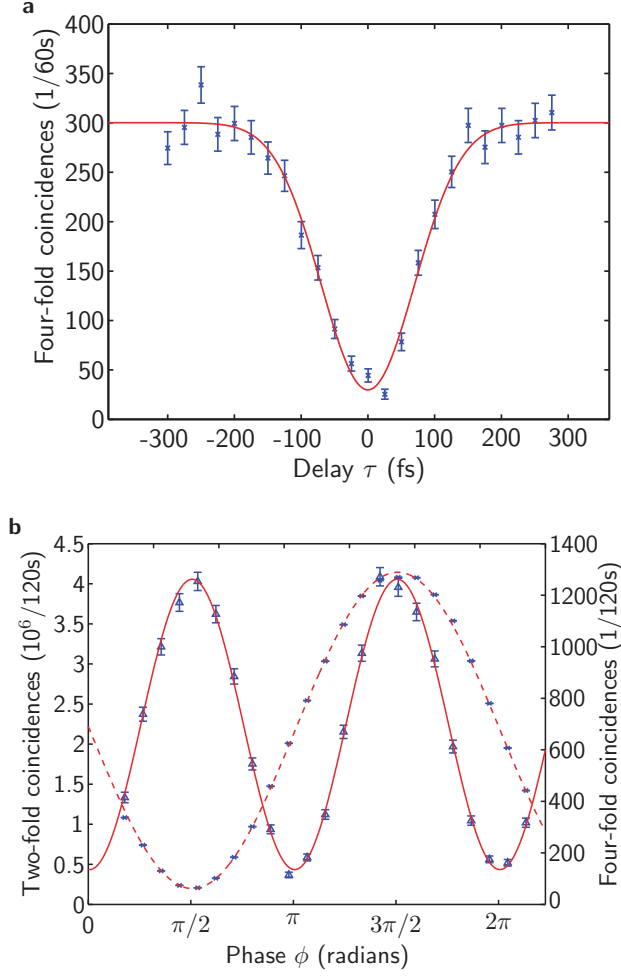
FIG. 2: **Quantum intereference of heralded photonic states. a** Hong-Ou-Mandel interference between two heralded single photons as a function of the externally controlled delay, τ. **b** Setting τ to zero and scanning the PMZI phase shows two-photon (solid) and single-photon (dashed) interference. The two-photon fringes clearly exhibit super-resolution. Error bars in both plots are derived from Poissonian statistics and contributions from multiple PDC pair emissions are removed from the Hong-Ou-Mandel interference and the two-photon fringes.
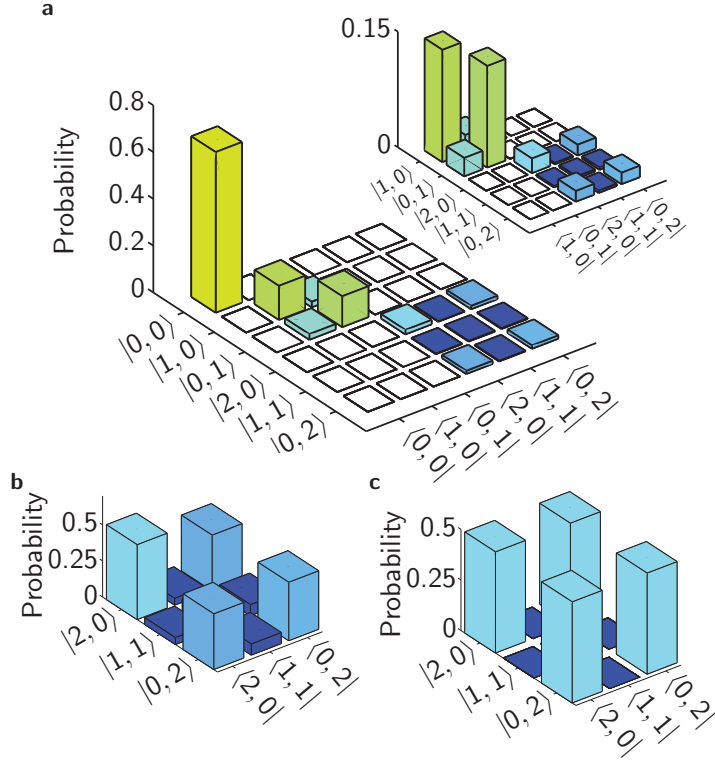
FIG. 3: **Reconstructed heralded quantum state. a** The full reconstructed state including vacuum, one-, and two-photon subspaces. (Inset) An enlargement of the one- and two-photon subspaces. **b** An enlargement of the two-photon subspace with elements normalized so that the trace is unity. **c** The ideal two-photon HB state. In all density matrices, $|m, n\rangle$ denotes m diagonally ($+45°$) polarised photons and n anti-diagonally ($-45°$) polarised photons. Bars are colored according to their magnitude.